Atmos. Chem. Phys. Discuss., 14, 15283–15322, 2014
www.atmos-chem-phys-discuss.net/14/15283/2014/
doi:10.5194/acpd-14-15283-2014

Atmospheric Chemistry and Physics Discussions

Aqueous phase oligomerization of methyl vinyl ketone through photooxidation – Part 1: Aging processes of oligomers

P. Renard[1], F. Siekmann[1], G. Salque[2], A. Smaani[1], C. Demelas[1], B. Coulomb[1], L. Vassalo[1], S. Ravier[1], B. Temime-Roussel[1], D. Voisin[2], and A. Monod[1]

[1]Aix-Marseille Université, CNRS, LCE FRE 3416, 13331, Marseille, France
[2]Université Joseph Fourier, Grenoble 1/CNRS-INSU, Laboratoire de Glaciologie et Géophysique de l'Environnement, 54 rue Molière, 38402 Saint-Martin-d'Hères, France

Received: 11 April 2014 – Accepted: 8 May 2014 – Published: 12 June 2014

Correspondence to: P. Renard (pascal.renard@etu.univ-amu.fr)

Published by Copernicus Publications on behalf of the European Geosciences Union.

Abstract

Secondary organic aerosol (SOA) represents a substantial part of organic aerosol, which affects climate and human health. It is now accepted that one of the important pathways of SOA formation occurs via aqueous phase chemistry in the atmosphere. Recently, we have shown in a previous study (Renard et al., 2013) the mechanism of oligomerization of MVK (methyl vinyl ketone), and suggested that unsaturated water soluble organic compounds (UWSOC) might efficiently form SOA in wet aerosol particles, even for weakly soluble ones like MVK. The atmospheric relevance of these processes is explored by means of process model studies (in a companion paper). In the present study we investigate the aging of these aqueous phase MVK-oligomers (Part 1).

We compared aqueous phase composition and SOA composition after nebulization, mainly by means of UPLC-ESI-MS and AMS, respectively. Both instruments match and show similar trend of oligomer formation and aging. The SMPS analysis performed on the nebulized solutions allow to quantify these SOA and to measure their mass yields.

We have highlighted in the current study that MVK $^{\bullet}$OH-oxidation undergoes kinetic competition between functionalization and oligomerization. The SOA composition and its evolution highly depend on the precursor initial concentration. We determined the threshold of MVK concentration, i.e. 2 mM, from which oligomerization prevails over functionalization. Hence, at these concentrations, $^{\bullet}$OH-oxidation of MVK forms oligomers that are SV-OOA, with low O/C and high f_{43}. Oligomers are then fragmented, via unidentified intermediates that have the properties of LV-OOA which then end into succinic, malonic and oxalic diacids. For lower initial MVK concentrations, the oligomerization is not the major process, and functionalization dominates, resulting in small carbonyls, dicarbonyls and mainly monoacids.

The aging of these oligomers could be an explanation for the presence of a part of the diacids observed in aerosol.

ACPD
14, 15283–15322, 2014

1 Introduction

Organic aerosol plays an important role in many atmospheric processes and has an important impact on climate and human health. Globally, about 20 % of the organic aerosol mass is emitted directly (Kanakidou et al., 2005; Spracklen et al., 2011), which conversely indicates the relevance of aerosol formed secondarily by transformation of organic gas phase species, i.e. secondary organic aerosol (SOA). The most commonly studied mechanism of SOA formation is the oxidation of volatile organic compounds (VOCs), which can lead to the formation of less volatile species that subsequently partition into the condensed phase (Donahue et al., 2011; Kanakidou et al., 2005; Kroll and Seinfeld, 2008; Hallquist et al., 2009). Nevertheless, the oxidation of VOCs also results in more water soluble products that readily partition into the aqueous phase (Blando and Turpin, 2000; Ervens et al., 2011; Epstein et al., 2013). Due to further reactivity in the liquid phase, higher molecular weight and less volatile compounds can be formed, which can remain at least in part in the condensed phase upon water evaporation, thus leading to additional secondary organic aerosol formation through aqueous phase reactions (aqSOA) (El Haddad et al., 2009; Carlton et al., 2009; Ervens et al., 2011; Ortiz-Montalvo et al., 2012). In particular, Lee et al. (2012) observed a significant enhancement of organic mass during the initial stage of oxidation of cloud water organics, that they explained by functionalizing dissolved volatile organics via hydroxyl radical ($^{\bullet}$OH) oxidation. Aqueous phase processes can be very different from those in the gas phase, thus leading to aqSOA with likely very different physical and chemical properties (Ervens et al., 2011; Ortiz-Montalvo et al., 2012). These differences can explain that the oxidation state of SOA formed during dry smog chamber experiments is significantly lower than that of ambient SOA (Kroll and Seinfeld, 2008; Aiken et al., 2008; De Carlo et al., 2008; Ng et al., 2010; Lee et al., 2012).

Volkamer et al. (2007) suggested that chemical processes in the aqueous phase of hygroscopic particles (wet aerosol) can efficiently contribute to aqSOA mass. Besides, wet aerosol provides higher precursor concentrations than in cloud and fog

ACPD
14, 15283–15322, 2014

water droplets and reside in the atmosphere over hours or days (Ervens et al., 2011), suggesting a significant role for aqSOA formation in wet aerosol, in particular, in regions with high relative humidity (Carlton and Turpin, 2013). Isoprene has the largest global atmospheric emissions (estimated at $\sim 600\,\mathrm{Tg\,yr^{-1}}$ Guenther et al., 2006) of all non-methane VOCs. Its key oxidation products, i.e. methacrolein (MACR) and hydroperoxides (Kroll et al., 2006) are known to contribute directly to the formation of SOA in the atmosphere. Methyl vinyl ketone (MVK) is the other main gas-phase oxidation products of isoprene (yielding from 32 to 44 %, Lee et al., 2005; Kroll et al., 2006). Unlike MACR, MVK does not lead to the formation of SOA during its gas phase photooxidation (Kroll et al., 2006; Surratt et al., 2006), likely because of the lack of an aldehydic hydrogen which precludes the formation of acidic products such as 2,3-dihydroxymethacrylic acid (i.e. 2-methylglyceric acid: 2-MG) for further particle-phase esterification reactions (Surratt et al., 2006). However, these results were obtained in smog chamber experiments performed under dry conditions where aqueous phase processes were excluded.

The photooxidation of carbonyl compounds linked to isoprene reactivity has been studied in the aqueous phase, and their ability to form oligomers and potentially aqSOA was shown (Altieri et al., 2006, 2008; Carlton et al., 2006, 2007; Perri et al., 2009; El Haddad et al., 2009; Tan et al., 2009, 2010; Zhang et al., 2010; Liu et al., 2012; Ortiz-Montalvo et al., 2012; Lim et al., 2013; Renard et al., 2013). In particular, Renard et al. (2013) showed that $^{\bullet}$OH oxidation of MVK in the aqueous phase proceeds via a radical mechanism leading to oligomers which molecular masses increase with the precursor initial concentration; and Liu et al. (2012) showed the ability of the generated oligomers to form SOA after water evaporation. It is thus likely that the atmospheric impact of MVK reactivity, and especially its ability to form SOA, is very different under dry and humid conditions.

The aim of the present study is to investigate the aging of the oligomers formed through aqueous phase photooxidation of MVK. We determine the SOA chemical composition during the formation and aging of the aqueous phase oligomers and we revisit

ACPD
14, 15283–15322, 2014

the corresponding SOA yields, under a large range of initial precursor concentrations (from 0.2 to 20 mM). Considering MVK as a proxy for unsaturated water soluble organic compounds (UWSOC), these concentrations are atmospherically relevant, in particular in wet aerosols (Ervens et al., 2011; Renard et al., 2013). In a companion paper (Ervens et al., 2014), we will discuss the explicit chemical mechanism of oligomer formation (as described in Renard et al., 2013) and loss and explore the atmospheric relevance of these processes by means of process model studies.

2 Experimental

A photoreactor was used to simulate the aqueous phase photooxidation of MVK. $^{\bullet}OH$ radicals were generated from H_2O_2 photolysis (Table 1). The liquid phase was analyzed using ultra-performance liquid chromatography mass spectrometry (UPLC-ESI-MS), ionic chromatography mass spectrometry (IC-ESI-MS), a total organic carbon (TOC) analyzer and liquid chromatography UV absorbance spectroscopy (UPLC-UV).

For aerosol generation, aliquots of the solution were sampled from the photoreactor at specific reaction times, then nebulized and dried prior to aerosol characterization using a scanning mobility particle sizer (SMPS) and a high resolution time-of-flight aerosol mass spectrometer (AMS) from Aerodyne (Fig. 1). Each experiment (aqueous phase photooxidation and aerosol generation) was repeated at least once.

2.1 Photoreactor

The photoreactor set-up used was based on the one described by Renard et al. (2013). It was a 450 cm^3 Pyrex thermostated photoreactor, equipped with a 1000 Watt xenon arc lamp (LSH 601, Oriel). A glass filter (ASTM 892 AM 1.5 standard) was used to remove the UV irradiation below 300 nm, resulting in an irradiance spectrum comparable to that of the sun but approximately twice as intense.

ACPD
14, 15283–15322, 2014

All experiments were performed at 25 °C and started with irradiation of UHQ water (18.2 MΩ cm, Millipore), then H_2O_2 (30 %, non-stabilized, Acros) was introduced, and after 10 min of H_2O_2 photolysis, MVK (99 %, Sigma Aldrich) was introduced at time 0. The experimental conditions (Table 1) were chosen in order to be representative of cloud droplets or wet aerosol conditions, respectively.

Tan et al. (2010) and Renard et al. (2013) have shown the important impact of initial concentrations on oligomer formation. The experiments were thus carried out with various MVK initial concentrations, i.e., 0.2, 0.5, 2, 5 and 20 mM (corresponding to 9.6 to 960 mg C L^{-1}), (as in Renard et al., 2013) which can be regarded as representative of the total concentrations of UWSOC in fog droplets and wet aerosol (Herckes et al., 2013).

We kept the ratio ($\frac{[H_2O_2]_0}{[MVK]_0} = 20$) used in Renard et al. (2013), in order to favor $^{\bullet}OH$ reaction toward MVK over its reaction with H_2O_2 by more than 90 % (Liu, 2011). Under these conditions, $^{\bullet}OH$ concentrations range were estimated from 5.1×10^{-14} M to 3.5×10^{-14} M (depending on pH, from 6 to 3), which fall in the range of the estimated values for cloud and fog droplets (Herrmann et al., 2010; Ervens and Volkamer, 2010 and Arakaki et al., 2013).

2.2 Aqueous phase characterization

2.2.1 UPLC-ESI-MS analyses

Aliquots of the solution sampled from the photoreactor were analyzed for organic species using an ultra-high performance liquid chromatographic system coupled to a time of flight mass spectrometer equipped with an electrospray source and an ion mobility cell (Synapt-G2 HDMS, Waters). The mass spectrometer was used in its resolution mode, up to 18 000 FWHM (Full width at half maximum) at m/z 400 and allowed for the determination of elemental composition of some organic species.

ACPD
14, 15283–15322, 2014

All parameters used are detailed in Renard et al. (2013). Briefly, the chromatographic separations were carried out on an UPLC column (HSS T3 C18, 2.1 · 100 mm – 1.8 µm; Waters) at 40 °C. The mobile phases consisted in (A) 0.1 % formic acid in water (Biosolve, 99 %) and (B) acetonitrile (Biosolve, ULC/MS). The gradient elution was performed at a flow rate of 600 µL min^{-1} using 5 to 95 % of B within 7 min and held at 95 % of B for 1.5 min. The sample injection volume was 10 µL.

During each chromatographic run, leucine enkephalin (2 ng μL^{-1}, $C_{28}H_{37}N_5O_7$, Waters Q-ToF product) was used for lock-mass correction to obtain accurate masses for each organic component eluting from the column. Optimum ESI conditions were found using a 0.5 kV capillary voltage, 40 V sample cone voltage, 450 °C desolvation temperature, 120 °C source temperature, 20 L h^{-1} cone gas flow rate and 800 L h^{-1} desolvation gas flow rate.

All products were detected as their protonated molecules ($[M+H]^+$) or sodium adducts ($[M+Na]^+$) in the positive mode, and their deprotonated molecules ($[M-H]^-$) in the negative mode. Data were collected from m/z 50 to 1800 in both ionization modes.

2.2.2 UPLC-UV analyses

An ultra-high performance liquid chromatographic (UPLC) system (Accela 600 auto sampler, Accela 600 pump, ThermoScientific, San Jose, CA) coupled to a diode array detector (Accela 600 PDA detector; ThermoScientific, San Jose, CA) was used to monitor the concentrations of MVK and H_2O_2 sampled from the photoreactor. The LC separation was performed using a Hypersil GOLD column (100 × 2.1 mm–1.9 µm, ThermoScientific) at 40 °C and at a flow rate of 300 µL min^{-1}. The mobile phase was water/acetonitrile (98 : 2) (v/v) and the injection volume was set to 2 µL. The spectra were recorded from 200 to 360 nm.

H_2O_2 and MVK show, with two different retention time (0.5 and 1.8 min, respectively), an intense absorption band (K-band; $\pi \rightarrow \pi^*$ transition) measured at 211 nm for both and a weak absorption band (R-band; $n \rightarrow \pi^*$ transition) at 308 nm for MVK.

ACPD
14, 15283–15322, 2014

The absorption intensity at 211 nm was directly proportional to the H_2O_2 and the MVK concentrations during the reaction. Thus, the kinetics of MVK $^{\bullet}$OH-oxidation in the aqueous phase was easily monitored by the K-band absorption.

2.2.3 IC-ESI-MS analyses

Quantification of organic acids in the solutions was performed with an ion chromatography system (Dionex ICS3000, Sunnyvale, USA) driven by Chromeleon® software (6.80 version), composed of a SP-5 gradient pump, an AS40 autosampler, a CD25 conductivity detector and coupled to a Thermo Scientific Surveyor MSQ (Thermo Electron, USA) mass spectrometer (MS) operated in the negative electrospray ionization (ESI) mode. A 4 mm ASRS 300 electrolytic suppressor operated in external water mode (7 mL min^{-1}) was placed before the conductivity cell. An additional peristaltic pump was used during measurements to wash the entrance cone of the mass spectrometer with water at a flow rate of 0.4 mL min^{-1}. The chromatographic separations were carried out on an IonPac AS11-HC column 4 × 250 mm (Dionex) coupled to a guard column (Dionex AG11-HC, 4 × 50 mm). A 25 µL sample was injected automatically using a 25 µL loop injection valve. The analysis was performed at 35 °C, with a flow rate set at 0.8 mL min^{-1}. Eluent A (Ultra High Quality water) and eluent B (100 mM NaOH) were flushed with purified helium gas for 30 min and kept under nitrogen atmosphere during the procedure. Separation was carried out using the following gradient (min, B %): 0, 1 %; 12, 5 %; 30, 19 %; 40, 40 %, 50, 1 %. The analytes were monitored using the selected ion-monitoring (SIM) mode, and signal areas (counts min^{-1}) of each peak were used for quantification.

2.2.4 TOC analyses

A total organic carbon/total nitrogen (TOC/TN) analyzer (N/C2100S) with the non-purgeable organic carbon (NPOC) method was used to quantify the TOC in our samples. The NPOC method consists in pre-purging samples with oxygen and

ACPD
14, 15283–15322, 2014

pre-acidifying (at pH = 2 with HCl) to remove the inorganic carbon and purgeable organic carbon.

TOC is measured by injecting the sample into a heated combustion tube (800 °C) with an oxidation catalyst. The CO_2 produced is measured by a non-dispersive infrared (NDIR) gas analyzer. TN is measured in parallel using chemiluminescence detection (CLD).

The TOC measurements were coupled with preparative liquid chromatography to separate the oligomers from the small reaction products, in order to check for the SOA mass yields determinations (see Sect. 3.2.3).

2.3 Particle generation and characterization

For aerosol generation, 35 mL of the solution was sampled at specific reaction times (Table 1), and nebulized using a TSI 3079 atomizer with a flow rate of 3.5 L min^{-1} (Fig. 1). The generated droplet flow was led through a silica gel diffusion dryer and diluted with filtered ambient air (at 5 L min^{-1}, using a HEPA capsule filter). A small fraction of the sample ($\approx$ 0.4 L min^{-1}) was passed through a Nafion dryer (Permapure, model MD-110), before entering a small 100 mL glass mixing chamber and the on-line analytical devices. The obtained relative humidity was constant during all experiments at ca. 15 % measured at the entrance of the AMS (Fig. 1). The nebulization time for each sample was 30 min and, to ensure constant and reproducible aerosol generation, only the last 15 min of nebulization were employed for data analysis. To avoid memory effects, before each nebulization experiment, the system was flushed by nebulizing UHQ water for 30 min.

The number size distribution was measured using a SMPS (SMPS+C, Grimm) consisting of a differential mobility analyzer (L-DMA) and a condensation particle counter (CPC5.403). The analyzed particle size ranged from 11 to 1083 nm (scanned within 6 min and 43 s).

An AMS was used to measure the bulk chemical composition of the non-refractory submicron particulate matter (De Carlo et al., 2006; Canagaratna et al., 2007). The

ACPD
14, 15283–15322, 2014

instrument was used under standard conditions (vaporizer at 600 °C and electron ionization at 70 eV), in the high sensitivity V-mode. Each measurement point was averaged for 2 min and 40 s (MS- and PToF-cycle, 40 s each, 2 cycles per run). The standard fragmentation table with the corrected air fragment column for our carrier gas and the default values of relative ionization efficiency were used in the AMS data analysis (Squirrel 1.51H and the software PIKA 1.10H).

3 Results

3.1 Evidence for oligomer formation and aging

We compared aqueous phase composition and SOA composition after nebulization, mainly by means of UPLC-ESI-MS and AMS, respectively.

3.1.1 Aqueous phase analyses

For each experiment, the solution was directly monitored using UPLC-ESI-MS and UPLC-UV for reaction times up to 150 min (Table 1). This time was higher than the complete consumption of MVK in order to study the formation of oligomers and their aging processes, as illustrated in Fig. 2.

In good agreement with our previous results (Renard et al., 2013), after 5 min of reaction (experiment B), no significant formation of high molecular weight compounds (HMWC) is observed (Fig. 2b), whereas after 10 min of reaction, mass spectra show that oligomer systems were formed on the whole range of the investigated m/z (50–1200), with regular pattern of 70.042 amu, which corresponds to the exact mass of MVK. At 50 min the oligomerization climax is reached (Fig. 2c). We observe different series of MVK-oligomers, corresponding to different initiator radicals identified by Renard et al. (2013) under the same conditions. As an example, the molecular structure of the most intense series is given in Fig. 2c and highlighted in red in the mass spectrum.

ACPD
14, 15283–15322, 2014

At that time, 90 % of MVK is consumed. Finally, the intensities of all the oligomer series decrease simultaneously for all masses with no change in the oligomer pattern up to 90 min. From this reaction time, the mass spectra show a collapse of the regular pattern in both negative (Fig. 2d, 150 min) and positive modes, certainly corresponding to a drastic aging process in which oligomers form smaller molecules. This hypothesis is confirmed by a more global approach, using the AMS analysis of the SOA formed after nebulization.

3.1.2 Aerosol composition of SOA generated after nebulization

Under similar conditions, we verified in a previous study (Liu et al., 2012) that nebulization of the reacted solutions and subsequent aerosol particle drying processes induced negligible chemical transformations of the oligomers compared to the aqueous phase composition. It was thus meaningful to compare the compositions of aqueous phase and SOA after nebulization.

AMS spectra (Fig. 3) show two dominant fragments, m/z 43 and m/z 44 (thought to be predominantly $C_2H_3O^+$ and CO_2^+ for ambient OOA, respectively (Ng et al., 2010)). The time profiles of the AMS total organic mass and both fragments clearly show (Fig. 3) the same three-step kinetic behavior as the one described above in Sect. 3.1.1 for the corresponding solutions (Fig. 2). Until 10 min of reaction, the intensity of the AMS total mass stays low (Fig. 3a) and the normalized mass spectrum at 5 min (Fig. 3b) is not significantly different from the one obtained by nebulizing an aqueous solution containing the reactants before reaction, with m/z fragments lower than 100. Then, the AMS total mass increases to reach a climax at 50 min (Fig. 3c), an order of magnitude higher than at 5 min. The mass spectrum is dominated by m/z 43 fragment (Fig. 3c). This observation is likely due to fragmentation (by electronic impact of the AMS, Ng et al., 2010) of oligomers containing repetitive carbonyl functions such as those identified in the aqueous phase (see the example of the molecular structure in Fig. 2c, and in Renard et al., 2013). Finally, the intensity of both the total organic mass and that of m/z 43 fragment decrease, the one of m/z 43 increases, and they both dominate

ACPD
14, 15283–15322, 2014

the mass spectrum with the same intensity at the end of our investigation (150 min, Fig. 3d).

Furthermore, comparing the mass spectra between 50 and 150 min at higher masses (m/z 100–200) (Fig. 4), it is clear that at 50 min of reaction, the spectrum contains higher fragments than at 150 min. It is thus likely that the oligomers are being significantly photooxidized through a fragmentation mechanism that forms smaller acidic compounds, and it confirms the oligomer aging process suggested in Fig. 2. After 50 min, oligomer fragmentation prevails over oligomer formation.

Note that the overall collection efficiencies (CE) of the AMS in our experiments were smaller than 1 (0.07 to 0.21 related to the SMPS signal), mainly due to particle bounce at the vaporizer surface before volatilization and to the shape and size-dependent transmission of the aerodynamic lens (Liu et al., 2007; Docherty et al., 2013; Miyakawa et al., 2013). The variability of the CE (depending on size, shape and physical state and of the aerosol) did not allow us for a quantitative determination of the SOA mass via AMS in our system. For the quantitative study, we used the data provided by the SMPS analysis.

3.2 SOA mass

3.2.1 Quantitative study of SOA generated after nebulization

The oligomer formation and aging were also observed by the quantitative analyses performed with the SMPS on the nebulized solutions. For experiment B, Fig. 5a shows a continuously increasing number size distribution with reaction time from 5 to 150 min, with an increasing mode during the two first kinetic steps (up to 50 min), and a decreasing mode during the third one, which corresponds to oligomer aging. In order to determine the particle mass concentrations, we used the method described by Kuwata et al. (2012) (Eq. 1) to determine the density (ρ_{org}) of the SOA generated in our system

ACPD
14, 15283–15322, 2014

at each reaction time t,

$$\rho_{\mathrm{org},t}\,(\mathrm{g\,cm^{-3}}) = \frac{12 + 1 \times \left(\frac{\mathrm{H}}{\mathrm{C}}\right)_t + 16 \times \left(\frac{\mathrm{O}}{\mathrm{C}}\right)_t}{7.0 + 5.0 \times \left(\frac{\mathrm{H}}{\mathrm{C}}\right)_t + 4.15 \times \left(\frac{\mathrm{O}}{\mathrm{C}}\right)_t} \quad (1)$$

where $(\mathrm{O:C})_t$ and $(\mathrm{H:C})_t$ are elemental ratios at reaction time t, as determined by the AMS analysis of the SOA formed in our system. These ratios extend to the same ranges as those used by Kuwata et al. (2012), and the resulting particle densities are reported in Table 2 and Table 3. In particular, Table 2 shows a substantial change in the H/C (decrease) and O/C (increase) after 50 min of reaction (t_{max}, for which the maximum SOA mass is reached) for experiment B, denoting the oligomer aging and inducing an increase of the aerosol density.

Using these particle densities, the total mass concentrations were determined, and the time evolution of the resulting distribution particle mass concentrations is shown in Fig. 5b for experiment B. The blank signal was determined prior each individual experiment by nebulizing pure water samples and was subtracted in the results for the mass calculation. At the initial reaction time (0 min), the particle size distribution was determined by nebulizing an aqueous mixture of the reactants (using experiment B concentrations), it showed a mass concentration ($11.0 \pm 1.4\,\mu\mathrm{g\,m^{-3}}$) not statistically different from the one obtained by nebulizing pure water (assuming a density of $1.1\,\mathrm{g\,cm^{-3}}$). This confirms that the reactants are too volatile to form substantial amounts of organic aerosol by nebulization of the solution prior to reaction.

Confirming the UPLC-ESI-MS aqueous phase analyses and the AMS results, a three-step kinetic behavior is also observed on the SMPS total mass concentrations (Figs. 5b and 6). A slow increase is observed during the first step (0–10 min). Then oligomerization takes place corresponding to a fast increase of the SMPS mass, until 50 min. Finally, after this climax of oligomerization, a significant decrease of the SMPS mass is observed. This decrease may be related to the decrease in the particle size (Fig. 5a), which can be due to the decrease of the oligomer size, by fragmentation of

ACPD
14, 15283–15322, 2014

the oligomers. It is thus likely that the oligomer aging forms more volatile compounds that the SMPS does not measure. The high correlation between the total aerosol mass concentration and the consumed MVK observed in Fig. 6 from 0 to 50 min, allows for the determination of the SOA mass yield, as discussed in Sect. 3.2.3.

3.2.2 Influence of initial MVK concentrations

The influence of the initial aqueous phase concentration of MVK on the SOA formation was investigated over a wide range, i.e. from 0.2 to 20 mM (Table 1). Not surprisingly, Fig. 7 shows that the total aerosol mass concentration increases with increasing initial MVK concentration. This observation is in very good agreement with the influence of MVK initial concentration on the oligomerization process observed in the aqueous phase by Renard et al. (2013). For experiments D and E, corresponding to the lowest initial MVK concentrations, the SMPS and AMS signals were low, and they could be influenced by water impurities, whereas no such influence was observed for experiments A, B and C. This is why the signal obtained from the blank experiments was subtracted only for experiments D and E in Fig. 7. Moreover, Fig. 7 clearly shows a different kinetic behavior of the SOA mass concentration from the lowest initial concentration experiments (D and E), compared to the three highest ones (experiments A, B and C). For experiments A, B and C, the SOA mass concentration increases rapidly, reaches a maximum, and then decreases, while for experiments D and E, the signal slowly increases and does not reach a maximum. This particular evolution may be due to different chemical mechanisms occurring at different initial concentrations. We hypothesized the predominance of oligomerization at 2 mM initial concentration and above, this is further discussed in Sect. 4.

The continuous increase of the particle number (shown in Fig. 5a for experiment B) with reaction time was observed for all initial concentrations (experiments A to E), whereas the decrease of the size mode (in the number size distributions, after t_{max}) was observed for the three highest initial concentrations only (experiments A, B and C) and not for experiments D and E, i.e. only during oligomer aging.

ACPD
14, 15283–15322, 2014

Furthermore, studies on relevant mixtures of UWSOC are in progress and could contribute to this chemistry.

3.2.3 SOA mass yields

The SOA mass yields, Y_t, were calculated at each reaction time step t from Eq. (2).

$$Y_t = \frac{[\mathrm{SOA}]_{t,\mathrm{SMPS}}}{\Delta[\mathrm{MVK}]_t} \quad (2)$$

Where $[\mathrm{SOA}]_{t,\mathrm{SMPS}}$ is the formed SOA mass at reaction time t, measured by SMPS (in mg L^{-1} of evaporated water, considering the dilution flow and the transmission efficiency in our nebulizing system, see Supplement Table S1); and $\Delta[\mathrm{MVK}]_t$ is the consumed [MVK] in mg L^{-1} at reaction time t.

The yields obtained at $t_{\max}$ for experiments A, B and C are shown in Table 3. Although the total SOA mass (at $t_{\max}$) increases linearly with the initial concentration for these three different experiments, the yields are statistically identical as well as their H/C and O/C ratios. These results show that the SOA compositions (at $t_{\max}$) are likely similar under these three different initial conditions. Furthermore, the yields obtained at $t_{\max}$ were about the maximum yields for each condition, as it is shown in Table 2 for experiment B. However, the large uncertainties are due to the estimation of the transmission efficiency in our nebulizing system (Supplement Table S1).

In order to check for these yields' values, another method was tested for experiment A at 90 min of reaction (i.e. close to $t_{\max}$). Preparative chromatography was performed using UPLC, where small molecules were separated from the oligomers using a divert valve (at retention times lower than 2 min.). The solution containing oligomers was accumulated, concentrated and analyzed using a TOC analyzer. From the carbon mass, we deduced the total mass using the H/C and O/C ratios given by the AMS. The yield was then directly calculated from the total mass of sample (in mg L^{-1}) divided by the mass of consumed MVK at the same reaction time. A yield of 59 ± 5 % (in mass) was

ACPD
14, 15283–15322, 2014

obtained with this method at 90 min of reaction, thus statistically similar from the one obtained by the nebulizing method (7 ± 50 %) at t_{max}.

These yields are significantly higher than those obtained by Liu et al. (2012) who obtained yields up to 9.9 % under similar experimental conditions as ours. It is important to note that these values were obtained assuming that all the particle densities were 1 g cm^{-3} in Liu et al. (2012), and also the transmission efficiency of the nebulizing system was calibrated with NaCl only. We show in the present study that succinic acid or ammonium nitrate are more adequate for the calibration (Supplement Table S1). The nebulizing system was slightly different, with a teflon bag in Liu et al. (2012) that could enable (i) larger amounts of wall losses for organic particles as compared to the system presented here; but (ii) longer particle residence times, leaving more time for gas-particle equilibrium than in our system. However, the control experiment using preparative chromatography confirms the yield value obtained here, independent on the nebulizing system and its calibration. The different yields obtained here as compared to the study by Liu et al. (2012) can be explained by the different irradiation Xe lamp intensities used: 300 W in Liu et al., 2012, and 1000 W in the present study. We have verified, using a spectroradiometer (SR-501, LOT-Oriel), that these irradiation systems represent respectively roughly half and twice of the solar irradiance intensity at sea level, for a 48.3° zenith angle. Thus, the range of the yields obtained here and by Liu et al. (2012) may represent the yields in the highly variable irradiated atmosphere.

It is interesting to note that the yields and densities obtained in the present study are in the same range as those of a similar study with a different precursor, i.e. glycolaldehyde (Ortiz-Montalvo et al., 2012). They reported aqSOA yields for oxidation products of glycolaldehyde (1 mM) of 120 to 50 %, and they calculated densities of 1.3 to 1.6 g cm^{-3} (respectively, increasing with photooxidation).

ACPD
14, 15283–15322, 2014

4 Discussion

4.1 MVK functionalization vs. oligomerization: influence of initial concentration

The two dominant AMS fragments m/z 44 (CO_2^+) and m/z 43 (mostly $C_2H_3O^+$) observed in our study, were used for a comparison with the aging of organic aerosol in the atmosphere compiled by Ng et al. (2010). In the latter study, low volatility oxygenated organic aerosol (LV-OOA) has higher f_{44} (ratio of m/z 44 to total organic aerosol) than semi-volatile oxygenated organic aerosol (SV-OOA) which in turn has higher f_{43} values (ratio of m/z 43 to total organic aerosol). Figure 8 compares our f_{44} vs. f_{43} values to those provided in the compilation by Ng et al. (2010). It is clear from this figure that the SOA composition and its evolution highly depend on the initial MVK concentration. For the three highest initial concentrations (experiments A, B and C), oligomerization took place with the formation of oligomers containing repetitive carbonyl functions such as those identified in the aqueous phase (Fig. 2c), inducing an important increase of f_{43} and a simultaneous decrease of f_{44}, roughly up to t_{max}. After t_{max}, most of the initial MVK is consumed, slowing down the oligomerization process, and an important decrease of f_{43} and a simultaneous increase of f_{44} is observed, likely due to oligomer aging, as detailed (for experiment B) in Sect. 3.1. At lower initial MVK concentrations (experiments D and E), oligomerization seems much less important and oxidation is the dominant process, as evidenced by the continuous increase of f_{44}. It can thus be suggested that, at these lower initial concentrations, functionalization dominates over oligomerization, and the aerosol is mainly composed of low-volatility organic acid and not of MVK-oligomers.

This observation is strengthened by the comparison of our results with those of previous studies. Zhang et al. (2010) performed aqueous phase $^{\bullet}OH$ oxidation of MVK (0.2 mM initial concentration), and observed the formation of functionalization products, i.e. formaldehyde, glyoxal, methylglyoxal, pyruvic, oxalic, formic, acetic, and malonic acids. Furthermore, for experiments D and E ($[MVK]_0 \leq 0.5$ mM), our f_{44}–f_{43} plots are similar to those obtained using a similar set-up, starting from pinonic acid, glyoxal

ACPD
14, 15283–15322, 2014

and glyoxylic acid at similar and higher initial concentrations (Lee et al., 2011a, b). In particular, starting at 3 mM of glyoxal, Lee et al., 2011b, obtained similar f_{44}–f_{43} plots as our experiments performed at much lower initial concentrations ($[MVK]_0 \leq 0.5$ mM), thus showing that the concentration is not the only important parameter in oligomerization processes, but the chemical nature of the precursor is also fundamental.

MVK oligomerization occurs via saturation of the vinyl group (Renard et al., 2013). It is likely that conjugation with the carbonyl function reduces steric hindrance and hence facilitates the oligomerization in the aqueous phase compared to other molecules.

4.2 Oligomer aging processes

The Van Krevelen diagram (Fig. 9) shows a significant increase of O/C and a significant decrease of H/C with reaction time after t_{max}. When oligomerization is the dominating process, almost no changes are observed in the van Krevelen diagram: the H/C and O/C values are confined in a restricted circle until t_{max}. The atomic ratios for H/C and O/C of MVK and the oligomers (with a degree of polymerization (DP) of 5) identified by Renard et al. (2013) are also reported in this diagram. MVK, oligomers and the nebulized solutions until t_{max} are confined in a circle that highlights the similarity of their structures.

After that time, the values of O/C (H/C respectively) increase (decrease respectively) out of the circle, thus denoting an oligomer aging process. Changes in functionality of organic aerosol are traced in this diagram along a line, which slope is −0.6. A very similar slope value (−0.5) was interpreted by Ng et al. (2011) as a COOH group addition to the site of a C-C bond cleavage, thus suggesting that the oligomer aging process proceeds via fragmentation. This is also suggested by the time evolution of the particle number size distributions (Fig. 5a: see Sect. 3.2.1). While a continuous increase of the particle number with reaction time was observed for all initial concentrations (experiments A to E), a significant decrease of the size mode was observed after t_{max} for the highest concentrations only (experiments A, B and C), i.e. during oligomer aging. This size mode decrease was also correlated with a decreasing total mass (Fig. 5b). These

ACPD
14, 15283–15322, 2014

observations, added to the fact that f_{44} increases during oligomer aging, indicate that the oligomer aging proceeds via fragmentation processes that generate smaller (or more volatile) and more acidic compounds.

The formation of carboxylic acids in the aqueous phase was monitored during the course of the reaction. In good agreement with Zhang et al. (2010), small volatile monocarboxylic acids such as acetic, formic and pyruvic acids were formed as primary reaction products from MVK reactivity. We further observed the formation of diacids as secondary or tertiary reaction products, such as oxalic, malonic, succinic (Fig. 10) malic and tartaric acids (not quantified). Finally, the formation of these diacids started at t_{max}, and was correlated to the increase of the AMS m/z 44 (CO_2^+) signal observed from the nebulized solutions. It is thus likely that the oligomer aging proceed via fragmentation (by $^{\bullet}$OH oxidation and/or photolysis), leading to the formation of smaller partially oxidized products (i.e. hydroxyacids or ketoacids such as those identified by Jaoui et al., 2006), which, in turn are oxidized into stable diacids.

5 Atmospheric implications

Figure 11 shows potential atmospheric fate of MVK in the aqueous phase. MVK $^{\bullet}$OH-oxidation undergoes kinetic competition between functionalization and oligomerization, depending on the precursor initial concentration. At 2 mM of MVK and above this concentration, oligomerization dominates over functionalization. Hence, at these concentrations, $^{\bullet}$OH-oxidation of MVK forms oligomers that are SV-OOA, with low O/C (lower than 0.50) and high f_{43}. Oligomers are then fragmented, via unidentified intermediates that have the properties of LV-OOA (with increasing O/C and decreasing H/C, Fig. 9) which then result in diacids. For lower initial MVK concentrations, the oligomerization is not the major process, and functionalization dominates, ending into small carbonyls, dicarbonyls and acids (Fig. 11).

Recently, we have shown in a previous study (Renard et al., 2013) the mechanism of oligomerization of MVK (methyl vinyl ketone), and suggested that UWSOC might

ACPD
14, 15283–15322, 2014

efficiently form SOA in wet aerosol particles, even for weakly soluble ones like MVK. This latter undergoes radical oligomerization, which is extremely fast and is able to form macromolecules as high as 1800 amu in polluted fogs and wet aerosols. Radical oligomerization occurs in wet aerosols and in most polluted fogs (Lim et al., 2013; Renard et al., 2013). This result, added to the fact that the lifetime of wet aerosols in the atmosphere are several days, suggests the relevance of radical oligomerization of UWSOC in the atmosphere. Besides, the aging of these oligomers could be an explanation for the presence of a part of the diacids observed in aerosol.

In Part 2 of this study, the atmospheric relevance of oligomerization will be explored by means of box model studies and comparison to other SOA formation pathways from MVK (and related compounds).

The Supplement related to this article is available online at doi:10.5194/acpd-14-15283-2014-supplement.

Acknowledgements. We thank the National Research Agency ANR (project CUMULUS ANR-2010-BLAN-617-01), AXA insurances, Région Rhone-Alpes (CIBLE program) and CNRS-INSU (LEFE-CHAT AtmOrbitrap project) for funding this research. We also thank B. Ervens (CIRES, University of Colorado, Boulder and Chemical Sciences Division, National Oceanic and Atmospheric Administration (NOAA), Boulder, CO, USA) for valuable scientific discussions on this topic.

References

Aiken, A. C., DeCarlo, P. F., Kroll, J. H., Worsnop, D. R., Huffman, J. A., Docherty, K., Ulbrich, I. M., Mohr, C., Kimmel, J. R., Sueper, D., Zhang, Q., Sun, Y., Trimborn, A., Northway, M., Ziemann, P. J., Canagaratna, M. R., Onasch, T. B., Alfarra, R., Prevot, A. S. H., Dommen, J., Duplissy, J., Metzger, A., Baltensperger, U., and Jimenez, J. L.: O/C and OM/OC ratios of primary, secondary, and ambient organic aerosols with high resolution time-of-flight

ACPD
14, 15283–15322, 2014

aerosol mass spectrometry, Environ. Sci. Technol., 42, 4478–4485, doi:10.1021/es703009q, 2008.
Altieri, K. E., Carlton, A. G., Lim, H. J., Turpin, B. J., and Seitzinger, S. P.: Evidence for oligomer formation in clouds: reactions of isoprene oxidation products, Environ. Sci. Technol., 40, 4956–4960, 2006.
Altieri, K. E., Seitzinger, S. P., Carlton, A. G., Turpin, B. J., Klein, G. C., and Marshall, A. G.: Oligomers formed through in-cloud methylglyoxal reactions: chemical composition, properties, and mechanisms investigated by ultra-high resolution FT-ICR mass spectrometry, Atmos. Environ., 42, 1476–1490, 2008.
Arakaki, T., Anastasio, C., Kuroki, Y., Nakajima, H., Okada, K., Kotani, Y., Handa, D., Azechi, S., Kimura, T., Tsuhako, A., and Miyagi, Y.: A general scavenging rate constant for reaction of hydroxyl radical with organic carbon in atmospheric waters, Environ. Sci. Technol., 47, 8196–8203, doi:10.1021/es401927b, 2013.
Blando, J. D. and Turpin, B. J.: Secondary organic aerosol formation in cloud and fog droplets: a literature evaluation of plausibility, Atmos. Environ., 34, 1623–1632, doi:10.1016/S1352-2310(99)00392-1, 2000.
Canagaratna, M. R., Jayne, J. T., Jimenez, J. L., Allan, J. D., Alfarra, M. R., Zhang, Q., Onasch, T. B., Drewnick, F., Coe, H., Middlebrook, A., Delia, A., Williams, L. R., Trimborn, A. M., Northway, M. J., DeCarlo, P. F., Kolb, C. E., Davidovits, P., and Worsnop, D. R.: Chemical and microphysical characterization of ambient aerosols with the aerodyne aerosol mass spectrometer, Mass Spectrom. Rev., 26, 185–222, 2007.
Carlton, A. G. and Turpin, B. J.: Particle partitioning potential of organic compounds is highest in the Eastern US and driven by anthropogenic water, Atmos. Chem. Phys., 13, 10203–10214, doi:10.5194/acp-13-10203-2013, 2013.
Carlton, A. G., Turpin, B. J., Lim, H., Altieri, K. E., and Seitzinger, S.: Link between isoprene and secondary organic aerosol (SOA): pyruvic acid oxidation yields low volatility organic acids in clouds, Geophys. Res. Lett., 33, L06822, doi:10.1029/2005GL025374, 2006.
Carlton, A. G., Turpin, B. J., Altieri, K. E., Seitzinger, S., Reff, A., Lim, H. J., and Ervens, B.: Atmospheric oxalic acid and SOA production from glyoxal: results of aqueous photooxidation experiments, Atmos. Environ., 41, 7588–7602, 2007.
Carlton, A. G., Wiedinmyer, C., and Kroll, J. H.: A review of Secondary Organic Aerosol (SOA) formation from isoprene, Atmos. Chem. Phys., 9, 4987–5005, doi:10.5194/acp-9-4987-2009, 2009.

ACPD
14, 15283–15322, 2014

DeCarlo, P. F., Kimmel, J. R., Trimborn, A., and Northway, M. J.: Field-deployable, high-resolution, time-of-flight aerosol mass spectrometer, Anal. Chem., 78, 8281–8289, 2006.
DeCarlo, P. F., Dunlea, E. J., Kimmel, J. R., Aiken, A. C., Sueper, D., Crounse, J., Wennberg, P. O., Emmons, L., Shinozuka, Y., Clarke, A., Zhou, J., Tomlinson, J., Collins, D. R., Knapp, D., Weinheimer, A. J., Montzka, D. D., Campos, T., and Jimenez, J. L.: Fast airborne aerosol size and chemistry measurements above Mexico City and Central Mexico during the MILAGRO campaign, Atmos. Chem. Phys., 8, 4027–4048, doi:10.5194/acp-8-4027-2008, 2008.
Docherty, K. S., Jaoui, M., Corse, E., Jimenez, J. L., Offenberg, J. H., Lewandowski, M., and Kleindienst, T. E.: Collection efficiency of the aerosol mass spectrometer for chamber-generated secondary organic aerosols, Aerosol Sci. Tech., 47, 294–309, 2013.
Donahue, N. M., Epstein, S. A., Pandis, S. N., and Robinson, A. L.: A two-dimensional volatility basis set: 1. organic-aerosol mixing thermodynamics, Atmos. Chem. Phys., 11, 3303–3318, doi:10.5194/acp-11-3303-2011, 2011.
El Haddad, I., Yao Liu, Nieto-Gligorovski, L., Michaud, V., Temime-Roussel, B., Quivet, E., Marchand, N., Sellegri, K., and Monod, A.: In-cloud processes of methacrolein under simulated conditions – Part 2: Formation of secondary organic aerosol, Atmos. Chem. Phys., 9, 5107–5117, doi:10.5194/acp-9-5107-2009, 2009.
Epstein, S. A., Tapavicza, E., Furche, F., and Nizkorodov, S. A.: Direct photolysis of carbonyl compounds dissolved in cloud and fog droplets, Atmos. Chem. Phys., 13, 9461–9477, doi:10.5194/acp-13-9461-2013, 2013.
Ervens, B. and Volkamer, R.: Glyoxal processing by aerosol multiphase chemistry: towards a kinetic modeling framework of secondary organic aerosol formation in aqueous particles, Atmos. Chem. Phys., 10, 8219–8244, doi:10.5194/acp-10-8219-2010, 2010.
Ervens, B., Turpin, B. J., and Weber, R. J.: Secondary organic aerosol formation in cloud droplets and aqueous particles (aqSOA): a review of laboratory, field and model studies, Atmos. Chem. Phys., 11, 11069–11102, doi:10.5194/acp-11-11069-2011, 2011.
Ervens, B., Wang, Y., Eagar, J., Leaitch, W. R., Macdonald, A. M., Valsaraj, K. T., and Herckes, P.: Dissolved organic carbon (DOC) and select aldehydes in cloud and fog water: the role of the aqueous phase in impacting trace gas budgets, Atmos. Chem. Phys., 13, 5117–5135, doi:10.5194/acp-13-5117-2013, 2013.
Ervens, B., Renard, P., Ravier, S., Clément, J.-L., and Monod, A.: Aqueous phase oligomerization of methyl vinyl ketone through photooxidation – Part 2: Development of the chemi-

ACPD
14, 15283–15322, 2014

cal mechanism and atmospheric implications, Atmos. Chem. Phys. Discuss., in preparation, 2014.
Guenther, A., Karl, T., Harley, P., Wiedinmyer, C., Palmer, P. I., and Geron, C.: Estimates of global terrestrial isoprene emissions using MEGAN (Model of Emissions of Gases and Aerosols from Nature), Atmos. Chem. Phys., 6, 3181–3210, doi:10.5194/acp-6-3181-2006, 2006.
Hallquist, M., Wenger, J. C., Baltensperger, U., Rudich, Y., Simpson, D., Claeys, M., Dommen, J., Donahue, N. M., George, C., Goldstein, A. H., Hamilton, J. F., Herrmann, H., Hoffmann, T., Iinuma, Y., Jang, M., Jenkin, M. E., Jimenez, J. L., Kiendler-Scharr, A., Maenhaut, W., McFiggans, G., Mentel, Th. F., Monod, A., Prévôt, A. S. H., Seinfeld, J. H., Surratt, J. D., Szmigielski, R., and Wildt, J.: The formation, properties and impact of secondary organic aerosol: current and emerging issues, Atmos. Chem. Phys., 9, 5155–5236, doi:10.5194/acp-9-5155-2009, 2009.
Herckes, P., Valsaraj, K. T., and Collett, J. L.: A review of observations of organic matter in fogs and clouds: origin, processing and fate, Atmos. Res., 132–133, 434–449, 2013.
Herrmann, H., Hoffmann, D., Schaefer, T., Bräuer, P., and Tilgner, A.: Tropospheric aqueous phase free radical chemistry: radical sources, spectra, reaction kinetics and prediction tools, Chemphyschem, 11, 3796–3822, 2010.
Jaoui, M., Corse, E., Kleindienst, T. E., Offenberg, J. H., Lewandowski, M., and Edney, E. O.: Analysis of secondary organic aerosol compounds from the photooxidation of d-limonene in the presence of NO_x and their detection in ambient $PM_{2.5}$, Environ. Sci. Technol., 40, 3819–3828, doi:10.1021/es052566z, 2006.
Jimenez, J. L., Canagaratna, M. R., Donahue, N. M., Prevot, A. S. H., Zhang, Q., Kroll, J. H., DeCarlo, P. F., Allan, J. D., Coe, H., Ng, N. L., Aiken, A. C., Docherty, K. S., Ulbrich, I. M., Grieshop, A. P., Robinson, A. L., Duplissy, J., Smith, J. D., Wilson, K. R., Lanz, V. A., Hueglin, C., Sun, Y. L., Tian, J., Laaksonen, A., Raatikainen, T., Rautiainen, J., Vaattovaara, P., Ehn, M., Kulmala, M., Tomlinson, J. M., Collins, D. R., Cubison, M. J., Dunlea, E. J., Huffman, J. A., Onasch, T. B., Alfarra, M. R., Williams, P. I., Bower, K., Kondo, Y., Schneider, J., Drewnick, F., Borrmann, S., Weimer, S., Demerjian, K., Salcedo, D., Cottrell, L., Griffin, R., Takami, A., Miyoshi, T., Hatakeyama, S., Shimono, A., Sun, J. Y., Zhang, Y. M., Dzepina, K., Kimmel, J. R., Sueper, D., Jayne, J. T., Herndon, S. C., Trimborn, A. M., Williams, L. R., Wood, E. C., Middlebrook, A. M., Kolb, C. E., Baltensperger, U.,

ACPD
14, 15283–15322, 2014

and Worsnop, D. R.: Evolution of organic aerosols in the atmosphere, Science, 326, 5959, 1525–1529, doi:10.1126/science.1180353, 2009.
Kanakidou, M., Seinfeld, J. H., Pandis, S. N., Barnes, I., Dentener, F. J., Facchini, M. C., Van Dingenen, R., Ervens, B., Nenes, A., Nielsen, C. J., Swietlicki, E., Putaud, J. P., Balkanski, Y., Fuzzi, S., Horth, J., Moortgat, G. K., Winterhalter, R., Myhre, C. E. L., Tsigaridis, K., Vignati, E., Stephanou, E. G., and Wilson, J.: Organic aerosol and global climate modelling: a review, Atmos. Chem. Phys., 5, 1053–1123, doi:10.5194/acp-5-1053-2005, 2005.
Kroll, J. H. and Seinfeld, J. H.: Chemistry of secondary organic aerosol: formation and evolution of low-volatility organics in the atmosphere, Atmos. Environ., 42, 3593–3624, 2008.
Kroll, J. H., Ng, N. L., Murphy, S. M., Flagan, R. C., and Seinfeld, J. H.: Secondary organic aerosol formation from isoprene photooxidation, Environ. Sci. Technol., 40, 1869–1877, 2006.
Kuwata, M., Zorn, S. R., and Martin, S. T.: Using elemental ratios to predict the density of organic material composed of carbon, hydrogen, and oxygen, Environ. Sci. Technol., 46, 787–794, 2012.
Lee, A. K. Y., Herckes, P., Leaitch, W. R., Macdonald, A. M., and Abbatt, J. P. D.: Aqueous OH oxidation of ambient organic aerosol and cloud water organics: formation of highly oxidized products, Geophys. Res. Lett., 38, L11805, doi:10.1029/2011gl047439, 2011a.
Lee, A. K. Y., Zhao, R., Gao, S. S., and Abbatt, J. P. D.: Aqueous-phase OH oxidation of glyoxal: application of a novel analytical approach employing aerosol mass spectrometry and complementary off-line techniques, J. Phys. Chem. A, 115, 10517–10536, 2011b.
Lee, A. K. Y., Hayden, K. L., Herckes, P., Leaitch, W. R., Liggio, J., Macdonald, A. M., and Abbatt, J. P. D.: Characterization of aerosol and cloud water at a mountain site during WACS 2010: secondary organic aerosol formation through oxidative cloud processing, Atmos. Chem. Phys., 12, 7103–7116, doi:10.5194/acp-12-7103-2012, 2012.
Lee, W., Baasandorj, M., Stevens, P. S., and Hites, R. A.: Monitoring OH-initiated oxidation kinetics of isoprene and its products using online mass spectrometry, Environ. Sci. Technol., 39, 1030–1036, 2005.
Lim, Y. B., Tan, Y., and Turpin, B. J.: Chemical insights, explicit chemistry, and yields of secondary organic aerosol from OH radical oxidation of methylglyoxal and glyoxal in the aqueous phase, Atmos. Chem. Phys., 13, 8651–8667, doi:10.5194/acp-13-8651-2013, 2013.
Liu, P. S. K., Deng, R., Smith, K. A., Williams, L. R., Jayne, J. T., Canagaratna, M. R., Moore, K., Onasch, T. B., Worsnop, D. R., and Deshler, T.: Transmission efficiency of an

ACPD
14, 15283–15322, 2014

aerodynamic focusing lens system: comparison of model calculations and laboratory measurements for the aerodyne aerosol mass spectrometer, Aerosol Sci. Tech., 41, 721–733, doi:10.1080/02786820701422278, 2007.

Liu, Y.: Etudes des impacts de la réactivité en phase aqueuse atmosphérique sur la formation et le vieillissement des Aérosols Organiques Secondaires sous conditions simulées, Ph.D. thesis, Laboratoire de Chimie de l'Environnement, Aix-Marseille University, Marseille, France, 2011.

Liu, Y., Siekmann, F., Renard, P., El Zein, A., Salque, G., El Haddad, I., Temime-Roussel, B., Voisin, D., Thissen, R., and Monod, A.: Oligomer and SOA formation through aqueous phase photooxidation of methacrolein and methyl vinyl ketone, Atmos. Environ., 49, 123–129, doi:10.1016/j.atmosenv.2011.12.012, 2012.

Miyakawa, T., Matsuzawa, R., Katayama, M., and Takegawa, N.: Reconsidering Adhesion and Bounce of Submicron Particles Upon High-Velocity Impact, Aerosol Sci. Tech., 47, 472–481 doi:10.1080/02786826.2013.763895, 2013.

Ng, N. L., Canagaratna, M. R., Zhang, Q., Jimenez, J. L., Tian, J., Ulbrich, I. M., Kroll, J. H., Docherty, K. S., Chhabra, P. S., Bahreini, R., Murphy, S. M., Seinfeld, J. H., Hildebrandt, L., Donahue, N. M., DeCarlo, P. F., Lanz, V. A., Prévôt, A. S. H., Dinar, E., Rudich, Y., and Worsnop, D. R.: Organic aerosol components observed in Northern Hemispheric datasets from Aerosol Mass Spectrometry, Atmos. Chem. Phys., 10, 4625–4641, doi:10.5194/acp-10-4625-2010, 2010.

Ng, N. L., Canagaratna, M. R., Jimenez, J. L., Chhabra, P. S., Seinfeld, J. H., and Worsnop, D. R.: Changes in organic aerosol composition with aging inferred from aerosol mass spectra, Atmos. Chem. Phys., 11, 6465–6474, doi:10.5194/acp-11-6465-2011, 2011.

Ortiz-Montalvo, D. L., Lim, Y. B., Perri, M. J., Seitzinger, S. P., and Turpin, B. J.: Volatility and yield of glycolaldehyde SOA formed through aqueous photochemistry and droplet evaporation, Aerosol Sci. Tech., 46, 1002–1014, 2012.

Perri, M. J., Seitzinger, S. P., and Turpin, B. J.: Secondary organic aerosol production from aqueous photooxidation of glycolaldehyde: laboratory experiments, Atmos. Environ., 43, 1487–1497, 2009.

Renard, P., Siekmann, F., Gandolfo, A., Socorro, J., Salque, G., Ravier, S., Quivet, E., Clément, J.-L., Traikia, M., Delort, A.-M., Voisin, D., Vuitton, V., Thissen, R., and Monod, A.: Radical mechanisms of methyl vinyl ketone oligomerization through aqueous phase OH-

ACPD
14, 15283–15322, 2014

oxidation: on the paradoxical role of dissolved molecular oxygen, Atmos. Chem. Phys., 13, 6473–6491, doi:10.5194/acp-13-6473-2013, 2013.
Spracklen, D. V., Jimenez, J. L., Carslaw, K. S., Worsnop, D. R., Evans, M. J., Mann, G. W., Zhang, Q., Canagaratna, M. R., Allan, J., Coe, H., McFiggans, G., Rap, A., and Forster, P.: Aerosol mass spectrometer constraint on the global secondary organic aerosol budget, Atmos. Chem. Phys., 11, 12109–12136, doi:10.5194/acp-11-12109-2011, 2011.
Surratt, J. D., Murphy, S. M., Kroll, J. H., Ng, N. L., Hildebrandt, L., Sorooshian, A., Szmigielski, R., Vermeylen, R., Maenhaut, W., Claeys, M., Flagan, R. C., and Seinfeld, J. H.: Chemical composition of secondary organic aerosol formed from the photooxidation of isoprene, J. Phys. Chem. A, 110, 9665–9690, 2006.
Tan, Y., Perri, M. J., Seitzinger, S. P., and Turpin, B. J.: Effects of precursor concentration and acidic sulfate in aqueous glyoxal-OH radical oxidation and implications for secondary organic aerosol, Environ. Sci. Technol., 43, 8105–8112, 2009.
Tan, Y., Carlton, A. G., Seitzinger, S. P., and Turpin, B. J.: SOA from methylglyoxal in clouds and wet aerosols: measurement and prediction of key products, Atmos. Environ., 44, 5218–5226, 2010.
Volkamer, R., SanMartini, F., Molina, L. T., Salcedo, D., Jimenez, J., and Molina, M. J.: A missing sink for gas-phase glyoxal in Mexico City: formation of secondary organic aerosol, Geophys. Res. Lett., 34, L19807, doi:10.1029/2007GL030752, 2007.
Zhang, X., Chen, Z. M., and Zhao, Y.: Laboratory simulation for the aqueous OH-oxidation of methyl vinyl ketone and methacrolein: significance to the in-cloud SOA production, Atmos. Chem. Phys., 10, 9551–9561, doi:10.5194/acp-10-9551-2010, 2010.

ACPD
14, 15283–15322, 2014

Table 1. Experimental conditions of OH-oxidation of MVK in the aqueous phase. All experiments are performed at 25 °C. Time 0 corresponds to MVK injection in the photoreactor (Samples taken at 0, 5, 10, 15, 30, 50, 75, 105, 150 min).

Exp. Name	$[MVK]_0$ (mM)	$[H_2O_2]_0$ (mM)	MVK 90 % Consumption time (min)	Aqueous phase characterization	Aerosol Characterization after nebulization
A	20	400	120		
B	5	100	50	UPLC-ESI-MS	SMPS
C	2	40	30	UPLC-UV	AMS
D	0.5	10	25	IC-ESI-MS*	
E	0.2	4	20		

* IC-ESI-MS analysis are performed on exp. A and B.

ACPD
14, 15283–15322, 2014

Table 2. Characteristics of the aerosol formed from nebulized MVK-solutions at different reaction times for experiment B.

Reaction Time (min)	D_P (nm)[a]	N ($\times 10^3$ cm^{-3})[a]	H/C[b]	O/C[b]	ρ_{org} (g cm^{-3})[b, c]	M_{SMPS} (µg m^{-3})[a, d]	Yield (%)[a, d, e]
5	28.3 ± 0.7	90 ± 6	1.55 ± 0.02	0.28 ± 0.05	1.0 ± 0.2	10 ± 10	70 ± 80
15	38 ± 1	530 ± 30	1.55 ± 0.01	0.26 ± 0.01	1.1 ± 0.1	100 ± 20	90 ± 60
50	44 ± 1	860 ± 40	1.55 ± 0.01	0.29 ± 0.01	1.1 ± 0.1	240 ± 50	80 ± 50
105	37 ± 1	1200 ± 50	1.47 ± 0.01	0.42 ± 0.01	1.2 ± 0.2	220 ± 40	70 ± 40
150	35 ± 1	1310 ± 50	1.38 ± 0.01	0.57 ± 0.01	1.4 ± 0.2	200 ± 30	60 ± 40

Values are the average of [a] three consecutive SMPS measurements, and [b] five consecutive O/C and H/C AMS measurements, and uncertainties represent the corresponding standard deviation of these averages.
[c] Particle densities are calculated using the method by Kuwata et al. (2012), the associated uncertainties include the accuracy of ±12 % stated by these authors for Eq. (1).
[d] Mass concentration values include the corresponding aerosol densities.
[e] Yield values and associated uncertainties include dilution + transmission efficiency determined for the nebulizing system (see Supplement Table S1).

ACPD
14, 15283–15322, 2014

Table 3. Overview of aerosol properties and mass yields for different initial MVK concentrations.

Exp. Name	$[MVK]_0$ (mM)	t_{max} (min)[a]	ρ_{org} ($g\,cm^{-3}$)[b]	M_{SMPS} ($\mu g\,m^{-3}$)[b]	Yield (%)[b, c]	H/C[b]	O/C[b]
A	20	105	1.1 ± 0.1	900 ± 200	70 ± 50	1.54 ± 0.01	0.30 ± 0.01
B	5	50	1.1 ± 0.1	240 ± 50	80 ± 50	1.55 ± 0.01	0.29 ± 0.01
C	2	30	1.1 ± 0.1	100 ± 20	80 ± 60	1.55 ± 0.01	0.28 ± 0.01

[a] Values are given at t_{max}, corresponding to the maximum aerosol mass concentration.
[b] All values and associated uncertainties are calculated as indicated in Table 2.
[c] Including dilution + transmission efficiency (TE) in the nebulizing system; TE: 17.2 (±7.9) for $[MVK]_0$ = 2 – 20 mM determined from NH_4NO_3.

ACPD
14, 15283–15322, 2014

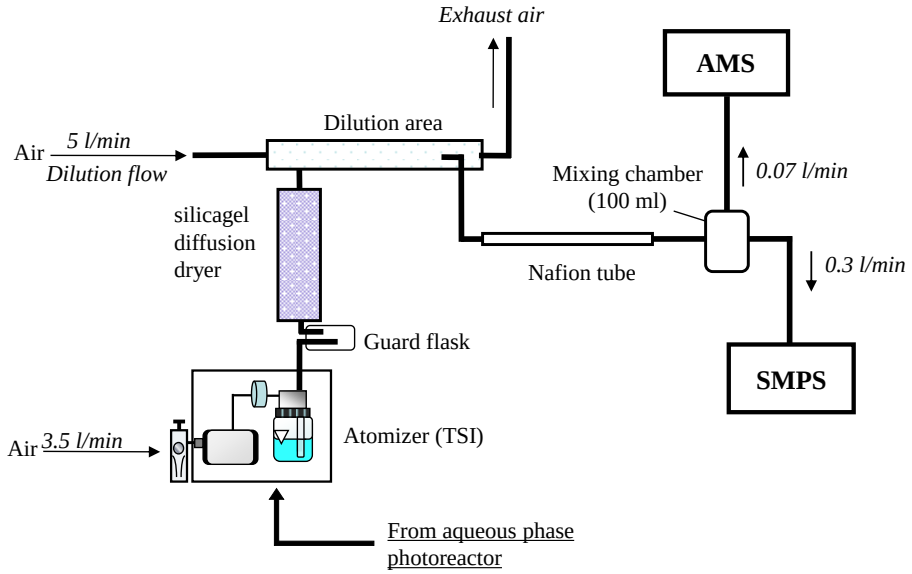

Figure 1. Schematic overview of the aerosol generation setup.

ACPD
14, 15283–15322, 2014

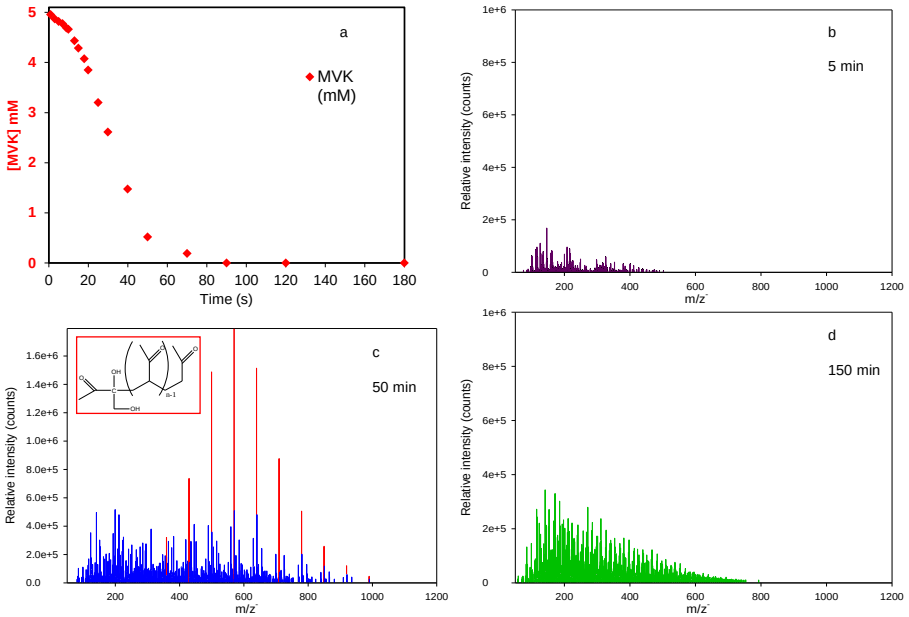

Figure 2. Time profiles of MVK concentrations during the reaction **(a)**, and the corresponding evolution of ESI-MS spectra for m/z 50–1200 (in the negative mode) at 5 min **(b)**, 50 min **(c)** and 150 min **(d)**. Highlighted in red, the most intense series of oligomers is presented in **(c)** together with its related molecular structure.

ACPD
14, 15283–15322, 2014

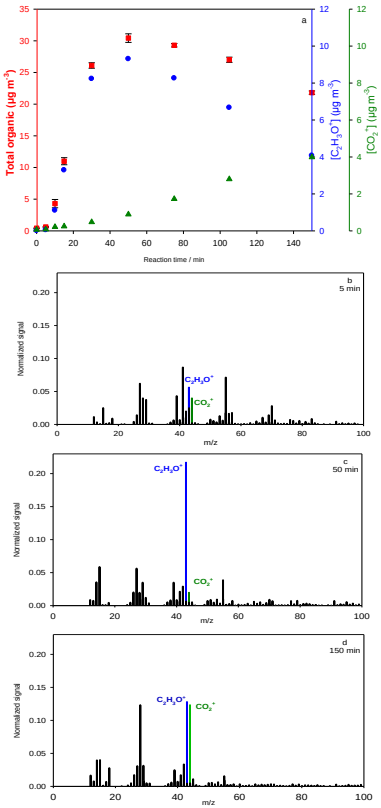

Figure 3. Time profiles of the AMS total organic mass (red), ion fragments $C_2H_3O^+$ at m/z 43 (blue) and CO_2^+ m/z 44 (green) for nebulized solutions from experiment B **(a)**, and the corresponding evolution of AMS mass spectra (for m/z 0–100) for nebulized solutions sampled after 5 min **(b)**, 50 min **(c)** and 150 min (**d)**. Values are averages of 5 consecutive AMS-runs, error bars represent their standard deviations.

ACPD
14, 15283–15322, 2014

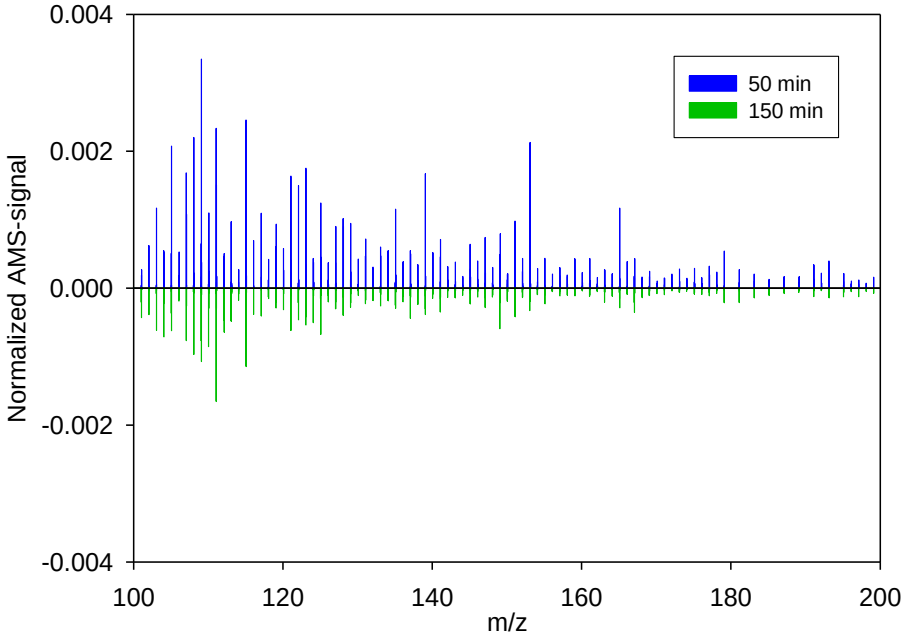

Figure 4. Comparison of AMS mass spectra (in the range 100–200 amu) of the nebulized solutions sampled from experiment B after 50 and 150 min of reaction in the aqueous phase.

ACPD
14, 15283–15322, 2014

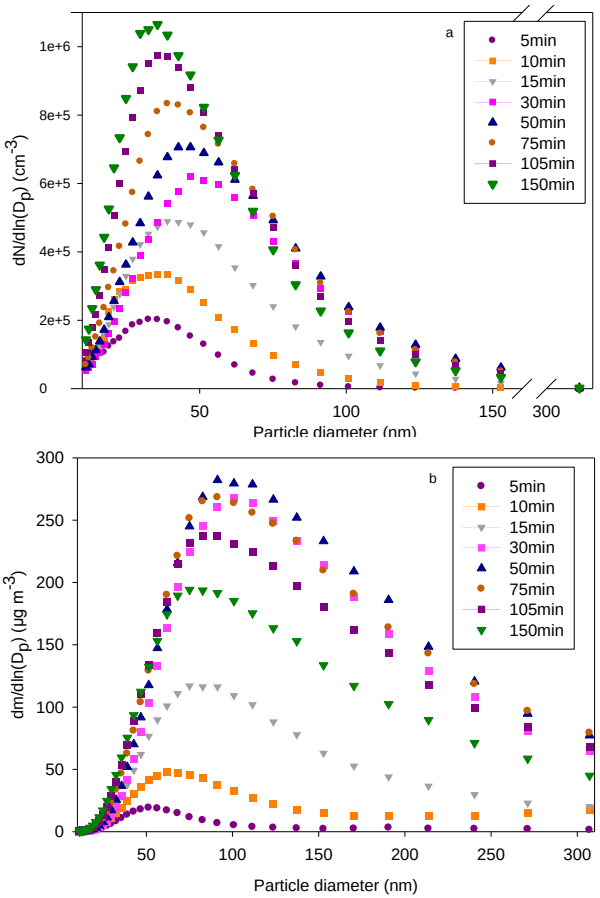

Figure 5. Evolution of particle number **(a)** and mass **(b)** size distributions for nebulized solutions sampled at different reaction times for experiment B.

ACPD
14, 15283–15322, 2014

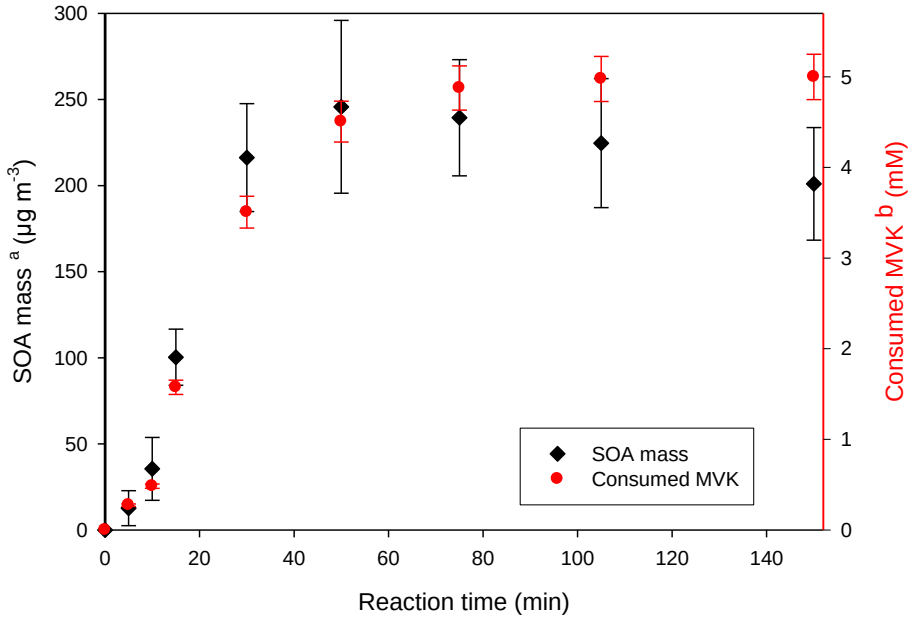

Figure 6. Time profiles of the total aerosol mass (black diamonds) from the nebulized solutions, and consumed MVK in the aqueous phase (red circles) for experiment B. [a] Values represent averages of three consecutive SMPS-measurements for each reaction time considering the corresponding density (Table 1). Error bars represent the sum of the standard deviation of these averages and the uncertainties of the density calculation. [b] MVK concentrations were determined by means of UPLC-UV, with an uncertainty of ±2 %.

ACPD
14, 15283–15322, 2014

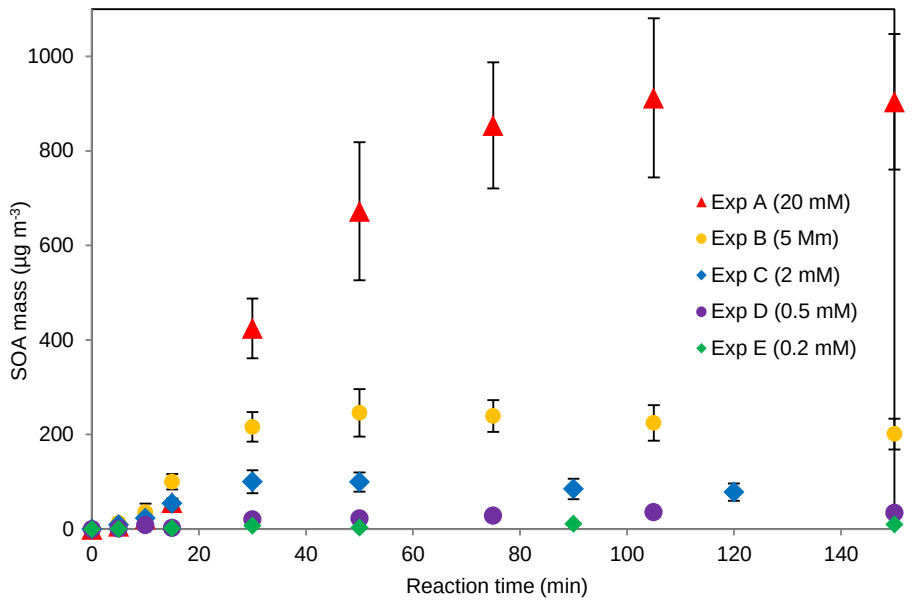

Figure 7. Influence of the initial MVK concentration on the evolution of the total SOA mass obtained from the nebulized solutions. Values represent averages of three consecutive SMPS-measurements for each reaction time considering the corresponding density (Table 3). Error bars represent the sum of the standard deviation of these averages and the uncertainties of the density calculation. For the lowest initial concentrations (experiments D and E), blank signals were subtracted, and a density of 1.1 g cm^{-3} was assumed.

ACPD
14, 15283–15322, 2014

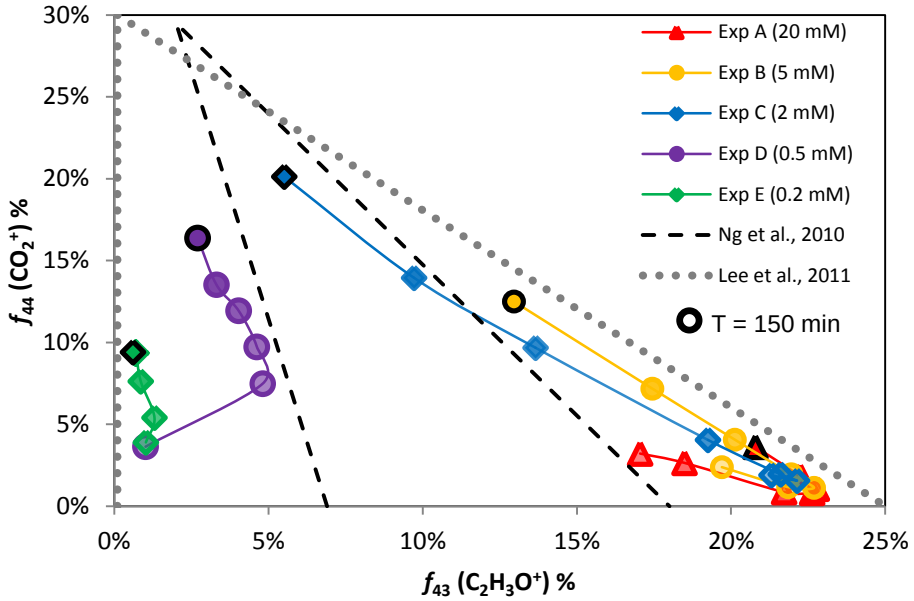

Figure 8. Fractions f_{44} vs. f_{43} for the nebulized solutions from experiments A, B, C, D and E, as measured by the AMS are compared to ambient air LV-OOA and SV-OOA from the compilation by Ng et al. (2010) (dashed black triangle), and are also compared to the nebulization data by Lee et al. (2011) (dotted grey triangle). For our experiments, the signal from blank experiments was subtracted. The data are shown for experiments A, B, and C from 10 to 150 min of reaction, and for experiments D and E from 15 to 150 min of reaction.

ACPD
14, 15283–15322, 2014

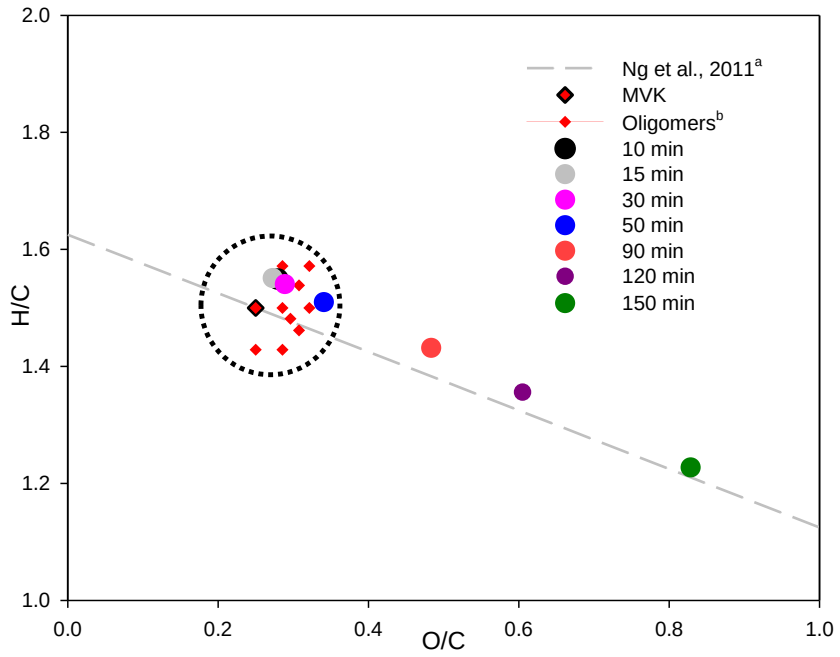

Figure 9. Van Krevelen diagram for the nebulized solutions of experiment C, as measured by the AMS. Only experiment C is shown for clarity as the data for experiments A and B are stacked together with the data shown. [a] Ng et al., 2011, for details see text Sect. 4.2. [b] Red diamonds represent the elemental ratios of oligomers with a Degree of Polymerization = 5 for the ten most abundant oligomer series identified by Renard et al. (2013). The black dotted circle highlights compounds with similar structures.

ACPD
14, 15283–15322, 2014

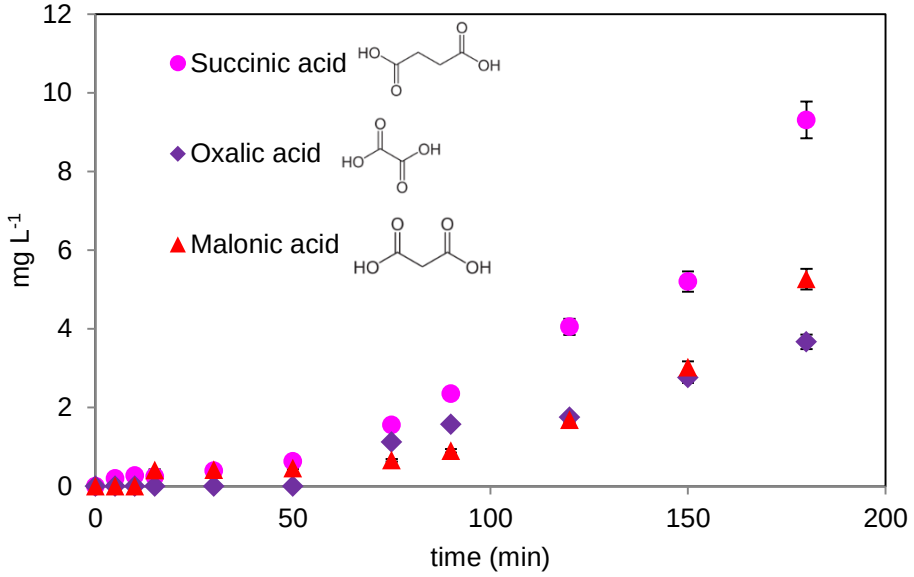

Figure 10. Time profiles of the quantified diacids in the solutions as measured by IC-ESI-MS for experiment B ($[MVK]_0 = 5$ mM).

ACPD
14, 15283–15322, 2014

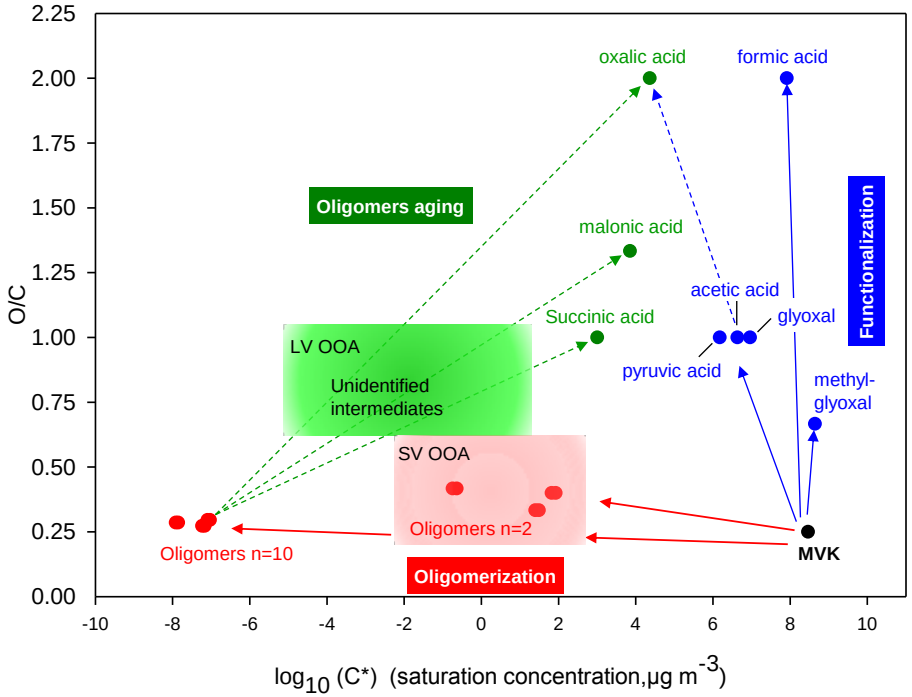

Figure 11. Potential atmospheric fate of MVK in the aqueous phase. X-Axis denotes volatility ($\log_{10}$ of C^* at 298 K), y-axis denotes oxidation state, approximated by O/C (Jimenez et al., 2009).

ACPD
14, 15283–15322, 2014